Desalination and Water Treatment
www.deswater.com

doi: 10.5004/dwt.2022.28688

267 (2022) 266–282
August

Low-cost *Liagora farinosa*/zeolite nanoporous composite for Congo red removal from wastewater

N.K. Soliman[a,*], Mohamed Shaban[b,c], Sayed A. Ahmed[d], Asmaa Ragab Dryaz[d], H.R. Abd El-Mageed[e], Refat El-Sayed[f,g], Esam S. Allehyani[f], Hamed M. Al-Saidi[f], Khaled N.M. Elsayed[h], Ahmed Hamd[a,b]

[a]*Basic Science Department, Faculty of Oral and Dental Medicine, Nahda University Beni-Suef (NUB), Beni Suef, Egypt, emails: nofal.khamis@nub.edu.eg (N.K. Soliman), ahmed.hamd@nub.edu.eg (A. Hamd)*
[b]*Nanophotonics and Applications Lab, Physics Department, Faculty of Science, Beni-Suef University, Beni Suef 62514, Egypt, email: mssfadel@aucegypt.edu*
[c]*Department of Physics, Faculty of Science, Islamic University of Madinah, Al-Madinah Al-Munawarah, 42351, Saudi Arabia*
[d]*Department of Chemistry, Faculty of Science, Beni-Suef University, Beni Suef 62511, Egypt, emails: Skader_70@yahoo.com (S.A. Ahmed), drasmaaragab505@gmail.com (A.R. Dryaz)*
[e]*Micro-Analysis, Environmental Research and Community Affairs Center (MAESC), Faculty of Science, Beni-Suef University, Beni-Suef, Egypt, email: dr_hamada33@yahoo.com*
[f]*Department of Chemistry, University College in Al-Jamoum, Umm Al-Qura University, Makkah, Saudi Arabia, emails: reabdelfattah@uqu.edu.sa (R. El-Sayed), esklehyani@uqu.edu.sa (E.S. Allehyani), hmsaidi@uqu.edu.sa (H.M. Al-Saidi)*
[g]*Chemistry Department, Faculty of Science, Benha University, Benha, Egypt*
[h]*Botany and Microbiology Department, Faculty of Science, Beni-Suef University, Beni-Suef 62511, Egypt, email: k.elsayed@science.bsu.edu.eg (K.N.M. Elsayed)*

Received 30 January 2022; Accepted 3 July 2022

ABSTRACT

A research plans comprising comprehensive analytical, laboratory, and field trials were successfully applied for precise exploration of a new facility to help in removing Congo red (CR) dye from industrial effluent effectively. Zeolite/algae (ZLF) nanocomposite was prepared by applying wet impregnation technique in order to incorporate one of the known Egyptian marine algae *Liagora farinosa* (LF) within the lattice of natural zeolite. Each of alga (LF), zeolite (Z) and ZLF nanocomposite were examined on the basis of structures, morphologies, and adsorption capacities using batch experiments to clarify the effect of different experimental factors on the ability of all adsorbents to capture CR dye from aqueous solutions. The preliminary results indicate superior adsorption capacity for the newly synthesized ZLF nanocomposite over Z and LF adsorbents, especially at lower CR dye concentrations. At pH 7 and 25°C, the maximum adsorption capacities were found to be 19.01, 11.23, and 8.1 mg/g for ZLF, LF, and Z, in the same order, which confirms results of the preliminary results on adsorption properties for the composite. Additionally, the Z, LF, and ZLF removal efficiency obtained from batch experiments were 65%, 84.21%, and 97.37% respectively. The ZLF nanocomposite newly synthesized in this study revealed a promising low-cost alternative adsorbent for holding and uptaking anionic dyes from industrial wastewater stream especially at low CR dye concentrations. The isotherms of dye adsorption on Z, LF, and ZLF were in well agreement with the Langmuir isotherm as well as pseudo-second-order kinetic model. In order to assess the sorption mechanism, Weber's intraparticle diffusion module was applied. The thermodynamic results showed that the adsorption of the CR dye onto Z, LF, and ZLF at 25°C is spontaneous, physical adsorption and exothermic

* Corresponding author.

1944-3994/1944-3986 © 2022 Desalination Publications. All rights reserved.

process. Finally, a real field sample was tested and the results revealed that the newly synthesized nanoadsorbent extracted dyes from industrial wastewater with a 90.97% efficiency, reaffirming the cornerstone of modern eco-friendly materials that aid in the reuse of industrial wastewater.

Keywords: *Liagora farinosa* (marine algae); Zeolite; Nanocomposite; Congo red dye; Adsorption; Wastewater treatment

1. Introduction

Dyes are produced annually worldwide with approximately 1.3 million tons according to one of the latest estimations. Nearly, 10,000 types of these dyes are utilized in an industrial level to produce different industrial products, which in turns causes a torrent of a significant amount of this pollutant into wastewater streams [1,2]. More precise estimate, revealed that from 40 to 65 L of wastewater is generated during 1 kg fabric production process. Thus, a noticeable amount of dye-rich wastewater is directly discharged into streams and/or rivers through aqueous effluent [3]. These kind of effluents compromise an issue that many of these dyes have a toxic nature even in low concentrations and have to be subjected to well-controlled operations. Dyes are generally classified regarding their reactivity and/or their charge into three classes: anionic: acid, direct and reactive dyes; cationic: basic dyes; and non-ionic: disperse dyes [4,5]. Anionic azo dyes compromise several structures from different dyes classes. The latter is well-known with its high toxicity and ingestion which can result in eye, skin, mucous membrane, and upper respiratory tract irritation; severe headaches; nausea; waterborne diseases [6]. Many years ago and until now azo dyes gathered great attention in various dyeing industries due to their high activity; therefore, these types of dyes generally represent nearly 50%–70% of the total dyes utilized by textile, plastic, and paper industries [2]. Congo red comes on the top of these dyes which composed of a benzidine-based diazo anionic dye with a complicated aromatic structure making it highly resistant to biodegradation. After leaching to the surrounding environment, it is metabolized into benzidine, a carcinogenic chemical for different organisms especially humans, which may cause some mutations and respiratory problems, threatening humans and aquatic animals [5,7]. Long-time subjection to Congo red may poison many organisms with a suspected carcinogen and mutagen [8]. Furthermore, its ability to affect directly on human health. For example; a weakened digestive system, appetite loss, and inflammation noticed to be common side effects for exposure to Congo red dye [9]. Flocculation, adsorption, Ion exchange, and ozonation, are all regarded as the most techniques widely used in dye removal [3,10–15]. Much more focus on adsorption as one of the smartest ways for improving quality of water [10,16–20]. Also bio sorbents including aquatic plant biomasses or fern are encouraged by several researchers for treating hazardous elements contaminating wastewater. Their non-hazardous nature, availability in huge quantities, good morphological properties, efficiency, and cost-effectiveness made them a perfect candidate [21,22]. The process of adsorption is reported as very vital technique as it is environmentally benign, cost-effective, functional, easy to test, and regeneration for the adsorbent [23]. Recently, synthetic adsorbents are introduced in order to obtain high quality purification for aquatic environment from harmful dyes and metals [24–27]. But due to their poisonous nature and pollution that may be directed to the environment, much more interest focused recently in colors and heavy metal removal using natural adsorbents such zeolite, algae, clay, rice husk, orange peel, and jujube stone [28–31]. Zeolite, the aluminosilicate clay mineral that occurs widely in nature can be applied in various purposes, including water purification and catalysis [32–34]. Because of its porosity and high surface area, zeolite possesses a considerable absorption capacity [20,35,36]. Zeolite is almost modified following the well-known techniques including dealumination, desilication, and templating [37,38]. In this research article, a comprehensive research plan comprising experimental, and field studies to explore the best adsorbent technology for effective uptaking and holding waste dyes, particularly Congo red (CR) dye, from industrial wastewater. The ability of *Liagora farinosa* (LF) to influence the adsorption capacity of Z was investigated by comparing the adsorption performance of Z, LF, and zeolite/algae (ZLF) nano-composite for CR dye removal from wastewater under various experimental settings. The novelty in this paper appears in the impact of natural alga LF on the performance of natural zeolite as an adsorbent besides the usage of an easy mixing and stirring impregnation method without a complicated chemical reaction or traditional nano structuring procedures to prepare a nanostructures composite. Z and LF were selected for this study for more than one reason, availability, natural occurrence, and affordability. Much more added values, the cost of Z, LF, and ZLF regeneration for reusability is considered much lower than many other adsorbents, which may play a major economic role in making this a viable dye removal option. In batch style tests, different variables including initial CR dye concentration, adsorbent dose, contact time, pH, and temperature were investigated on CR dye removal. Moreover, adsorption kinetics, isotherms, and thermodynamics were calculated from experimental results.

2. Materials and methods

2.1. Raw materials, dyes, and reagents

The (LF) alga sample was successfully collected from the inter-tidal area of Egyptian Red Sea shores near the distance between Marsa Alam and Quoseir cities. The collected parts of LF were carefully washed with tap and distilled water more than one time in order to remove the undesired materials and dried near room temperature. The air-dried alga was well-grinded by blender into a powder phase to increase its surface area. Congo red dye was purchased from Sigma-Aldrich (Cairo, Egypt) and dissolved in distilled water. Zeolite ore was given by El Nasr Company (Cairo, Egypt) for mining and utilized as is without further modification. Sigma-Aldrich (Cairo, Egypt) was selected to purchase the CR dye with high purity (99%). For pH correction, sodium

hydroxide granules with a purity of 99.99% and hydrochloric acid with a purity of 36% were purchased from Sigma-Aldrich (Cairo, Egypt).

2.2. Preparation of zeolite/algae composite

In the current research article wet impregnation technique was chosen in order to produce the zeolite/algae (ZLF) nanocomposite [39]. The procedure was as follows: in 20 mL distilled water 1 g of zeolite and 1 g of alga were mixed and stirred at 500 rpm for 60 min on a magnetic stirrer, then in ultra-sonicated for 60 min and repeated three times followed by filtration and washing with distilled water for several times, and finally dried using a vacuum oven at 60°C during 24 h. All adsorbents (Z, LF, and ZLF nanocomposite) under investigations in this study were subjected to different characterization techniques including Fourier-transform infrared spectroscopy (FTIR), X-ray diffraction (XRD), and field-emission scanning electron microscopy.

2.3. Preparation of the adsorbate

CR, which known as sodium salt of 3,30-([1,10-biphenyl]-4,40-diyl)bis(4-aminonaphthalene-1-sulfonic acid) and with general chemical formula: $C_{32}H_{22}N_6Na_2O_6S_2$ following the IUPAC system for nomenclature of organic compounds, is displayed in Fig. S1. A 1,000 mg/L stock solution was made by dissolving 1 g of CR dye in 1 L of distilled water. The stock solution was diluted using with distilled water to prepare the different working solutions with different concentrations. The pH of the working solutions was altered to 3, 5, 7, and 10 by adding either 0.1 M NaOH or 0.1 M HCl solutions.

2.4. Samples characterizations

The XRD measurements were carried out with an Empyrean PANalytical diffractometer that used a Cu $_{(K\alpha)}$ source with a wavelength of $\lambda\alpha$ = 0.154045 nm and operated at 40 kV, 35 mA with a scan step of 0.02° between 20° and 70°. The average crystallite sizes, D_s, of the produced nanoadsorbents, were calculated using the Scherer formula, $D_s = 0.94\ \lambda\alpha/\beta_w \cdot \text{Cos}\varphi$; where β_w and φ are the corrected full width at half maximum and diffraction angle, respectively [40]. Scanning electron microscopy (SEM) micrographs were measured using a Quanta FEG-250 microscope (Switzerland). A Bruker VERTEX 70 FTIR spectrophotometer (Billerica, Massachusetts, USA) was used to measure FTIR spectra using the dry KBr pellet technique.

2.5. Adsorption studies

Four adsorption experiment series shown in Table S1 were conducted on Z, LF, and ZLF adsorbents under different conditions of adsorption, including initial dye concentration, adsorption temperature, adsorbent dose, and initial pH of the solution. Batch mode style was chosen as a

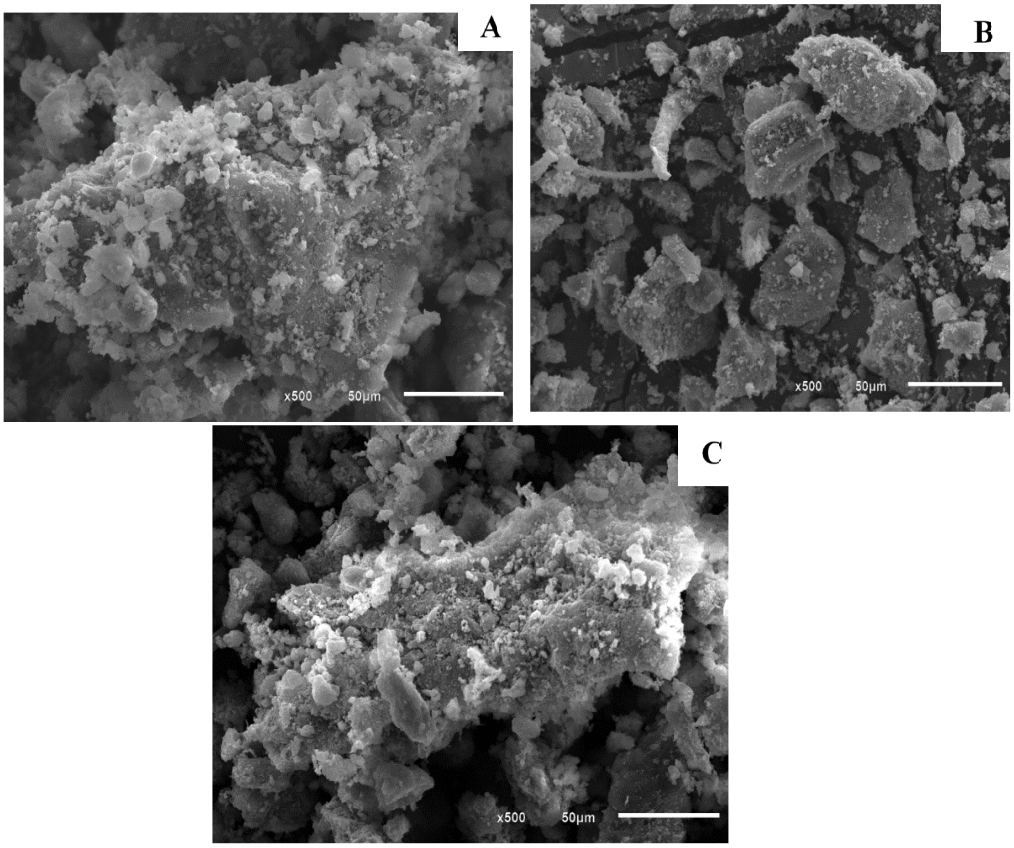

Fig. 1. SEM micrographs of (A) Z, (B) LF, and (C) ZLF adsorbents.

laboratory scale style for testing for all CR adsorption tests keeping in continuous shaking. The experimental variables such as dye starting concentrations (5–25 mg/L), adsorbent dose (0.01–0.05 g per 20 mL of CR solution), contact time (480 min), temperature (25°C–90°C), and pH 3–10. Each of time and solution volume were fixed to be 480 min and 20 mL respectively during the whole experiments. The variance in CR concentration was determined by following the absorption peak with a UV/Vis spectrophotometer. The reusability of Z, LF, and ZLF adsorbents was tested five times with 0.02 g of each, 20 mL of 10 mg/L beginning CR concentration, and 480 min contact time at 25°C and pH 7. After each run, the Z, LF, and ZLF adsorbents were removed from the solution, rinsed with DI water, and ready for the next run.

In order to calculate the amount of CR uptake by the synthesized nanocomposite at equilibrium q_e (mg/g) and time t (q_t), Eqs. (1) and (2) were used as well as the CR dye removal efficiency [41–43].

$$q_i = \left(C_o - C_i\right)\frac{V}{m};\ i = e,t \tag{1}$$

$$\text{CR dye removal \%} = \frac{\left(C_o - C_t\right)}{C_o} \times 100 \tag{2}$$

where C_o, C_t, and C_e are the concentrations of CR in mg/L at the start, after time t, and at equilibrium, respectively. V is the CR volume in mL and m is the Z, LF, and ZLF masses in mg. The presented results were the mean values of three independent experiments.

2.6. Adsorption isotherm

Each of Freundlich, Langmuir, and Temkin isotherms were used individually in order to explain isotherms of the reaction for the developed ZLF, LF, Z and nanocomposite for the tested CR [44–46]. All linear isotherm equations as well as their parameters are discussed in detailing in the supplemental data. Eq. (3) can be used to determine the degree of favorability of the Langmuir isotherm for equilibrium data using the value of the dimensionless separation factor (R_L) [47].

$$R_L = \frac{1}{\left(1 + K_L C_{\max}\right)} \tag{3}$$

where $C_{\max}$ denotes the maximum initial CR concentration.

2.7. Adsorption kinetics and mechanism

Theoretical calculations including intraparticle diffusion, pseudo-first-order, pseudo-second-order, and simple Elovich kinetic model were applied in order to identify the adsorption mechanisms as well as kinetics models that best match the adsorption of CR onto Z, LF, and ZLF adsorbents [48–50]. In the supplemental data, all linear kinetics equations and their parameters are discussed. In triplicates, the average values of all adsorption findings were measured. OriginPro 2018's statistical functions were used to calculate regression coefficients (R^2) for several kinetic and isotherm models.

2.8. Thermodynamic study

The adsorption of CR dye was studied at different temperature range of 20°C–90°C under constant pH of 7, concentration 10 mg/L and Z, LF, and ZLF adsorbents dose of 0.02 g per 20 mL of dye. Several thermodynamic parameters such as ΔG (Gibbs' free energy change), ΔH (enthalpy change) and the change in entropy (ΔS) were determined in order to understand the adsorption nature of dispersed red 60 dye. The thermodynamic parameters ΔG, ΔH and ΔS were calculated from the slope and intercept resulting from plotting of $1/T$ vs. $\ln k_c$ using Van't Hoff equation which can be represented by Eq. (4).

$$\ln k_c = \frac{\Delta S}{R} - \frac{\Delta H}{RT} \tag{4}$$

where $k_c = q_e/C_e$ and (ΔG) Gibbs' free energy change can be calculated using Eq. (5).

$$\Delta G = -RT \ln k_c \tag{5}$$

where T is the absolute temperature in K° and R is the universal gas constant (8.314 J/mol K).

2.9. Field experiments

The novel nanoadsorbent system newly fabricated in this study was subjected to a real case study and tested as an effective, environmentally acceptable adsorbent that could be used on a broad scale to remove industrial waste dye from wastewater. Wastewater containing waste dye was received from clothes dying plant in Beni-Suef City for this purpose and used as received without further treatment or dilution. The best adsorbent system was chosen based on our improved theoretical and experimental results.

3. Results and discussion

3.1. Adsorbent characterization

3.1.1. SEM characterization

Fig. 1 reveals the SEM photo-shots for each of Z, LF, and ZLF adsorbents. In Fig. 1A on the surface of the zeolite you we can notice that agglomerated rounded regular form particles, a rough surface, varied particle sizes, and porous spaces are very clear. While Fig. 1B displays the SEM photo-shots of LF, which reveals that LF has a less porous surface, which in turns impacts the surface area of LF and hence reduces its adsorption capacity. Following-up the changes demonstrated in Fig. 1C which indicate that treatment of zeolite with LF algae resulted in coating the pores on zeolite surfaces with LF particles and turned into agglomerated particles, as shown in the SEM photo-shots of the nanocomposite. The creation of the ZLF nanocomposite might be validated by comparing the morphological topographies of the nanocomposite to those of Z and LF.

Hydrodynamic diameter as well as particle size distribution of the nanoadsorpent under investigation (Z, LF, and ZLF) were calculated using DLS analyzer technique. The data obtained confirmed the nanostructure of all adsorbents at which Z, LF and ZLF showed particle sizes were 82.5, 90.4, and 89.1 nm in the same order. Moreover, Brunauer–Emmett–Teller surface areas were 91.6, 118.6, and 114.5 m^2/g, respectively.

3.1.2. X-ray diffraction characterization

XRD peaks of Z, LF, and ZLF adsorbents are demonstrated in Fig. 2A. The main XRD peaks that characterize natural zeolite minerals exist at 2θ of ~ 9.85°, 22.41°, 26.15°, 26.84°, 28.12°, 30.075°, and 32.04°, which are consistent with those described by other researchers [51,52]. The main zeolite peaks at 22.41° and 28.12° had *d*-spacing values of 3.96809 and 3.17323 Å. While the main XRD peaks of LF appear at about 26.11°, 27.14°, 29.80°, 31.59°, 33.03°, 36.00°, 37.81°, 38.30°, 42.84°, 45.77°, 48.25°, 50.10°, and 52.34°. Following-up the changes in XRD pattern of ZLF nanocomposite showed main characteristic peaks nearly at 9.87°, 11.14°, 22.40°, 26.21°, 27.23°, 29.92°, 31.99°, 33.12°, 36.11°, 37.85°, 38.59°, 45.91°, and 48.41°. The average crystallite sizes were calculated using the Scherer equation and were found to be 29.6, 42.7, and 63.9 nm for Z, LF, and ZLF, in order, which is considered a proof for the presence of the nanostructure nature of the newly synthesized composite.

3.1.3. FTIR analysis

The FTIR spectra of Z, LF, and ZLF nanoadsorbent are displayed in Fig. 2B. Generally, all broad bands in the FTIR spectrum appeared at 3,452; 3,432 and 3,442 cm^{-1} wavelenghts ascribed as the stretching hydroxyl (OH) group [53,54]. More specificity, peak appeared at 1,029 cm^{-1} related to vibration mode of Si–O–Al found in the structure of zeolite. The last mentioned peak was shifted to 1,039 cm^{-1} in case of ZLF [55], 603 cm^{-1} (Si–O–Al). While peak appared at 1,029 cm^{-1} belongs to octahedral aluminum (Al–OH•) [56], and the peak at 464 cm^{-1} belongs to the Si–O–Si bending of zeolite which was shifted to 461 cm^{-1} for ZLF [56]. All peaks that appeared in the region from 400 to 800 cm^{-1} belong to the metal oxides [57]. While, spectra obtaind from FTIR for LF algae revealed a band at 3,700 cm^{-1} characteristics of an amine group (–NH) stretching, the band at 3,422 cm^{-1} characteristics of a hydroxyl group (–OH) of phenolic groups. The peak at 2,935 cm^{-1} were allocated to the stretching vibration of alkyl (–CH) groups, while the peak located at 1,647 cm^{-1} was corresponding to (–C=O). The band at 1,475 cm^{-1} was attributed to the (C–H) band [58,59]. The sulfate group or the C–O bond may be responsible for the bands around 1,069 cm^{-1} [60], while the bands between 3,300 and 3,500 cm^{-1} are caused by amine N–H stretching vibrations, and the band around 2,915 cm^{-1} is caused by carboxylic group O–H stretching [61]. Either peak shift and/or peak disappearance agreed with the results from other characterization techniques, confirm that a novel compound with either chemical and/or physical bond has been formed. The positions of the distinctive FTIR bands for Z, LF, and ZLF adsorbents are listed in Table S2.

3.2. Factors influencing the adsorption process

3.2.1. Effect of initial CR dye concentration

The amount of dye disappeared from the solutions under test by adsorption is strongly dependent on the starting dye concentration. Fig. 3A–F illustrate the variations in the removal efficiency and amount of CR adsorbed using Z, LF, and ZLF adsorbents at varying beginning concentrations. Either the amount of dye removed and/or the dye removal efficiency were elivated during the first stage of the adsorption process, then a gradual decrease with noticed until equilibrium reached. Another noticable observation, that after equilibrium has been reached, contact time had no valuable effect on the adsorption process utilizing new sorbents. The rapid removal rate at this stage could be ascribed by the fact that the presence of a large number of uncovered active adsorption sites on the adsorbent's surface early in the adsorption process. This uncovered sites converted to be fully occupied by the adsorbed CR molecules as the time of contact between adsorbent and adsorbate increases, and the repulsion force that arises between the CR molecules

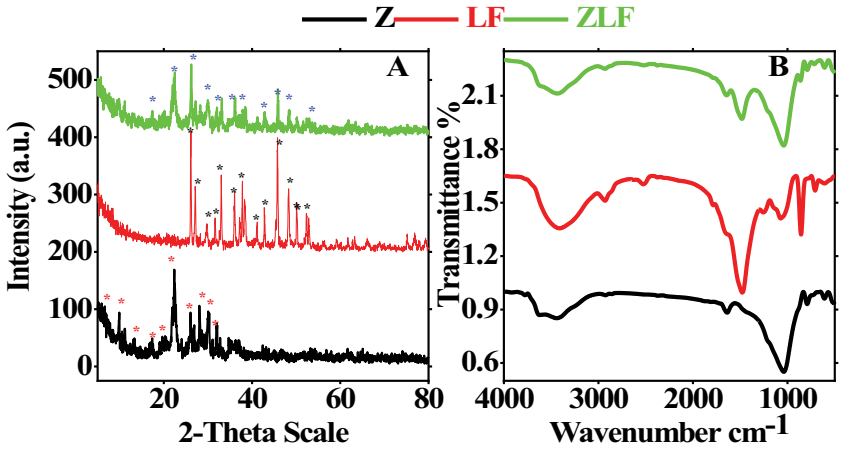

Fig. 2. (A) XRD and (B) FTIR charts of Z, LF, and ZLF adsorbents.

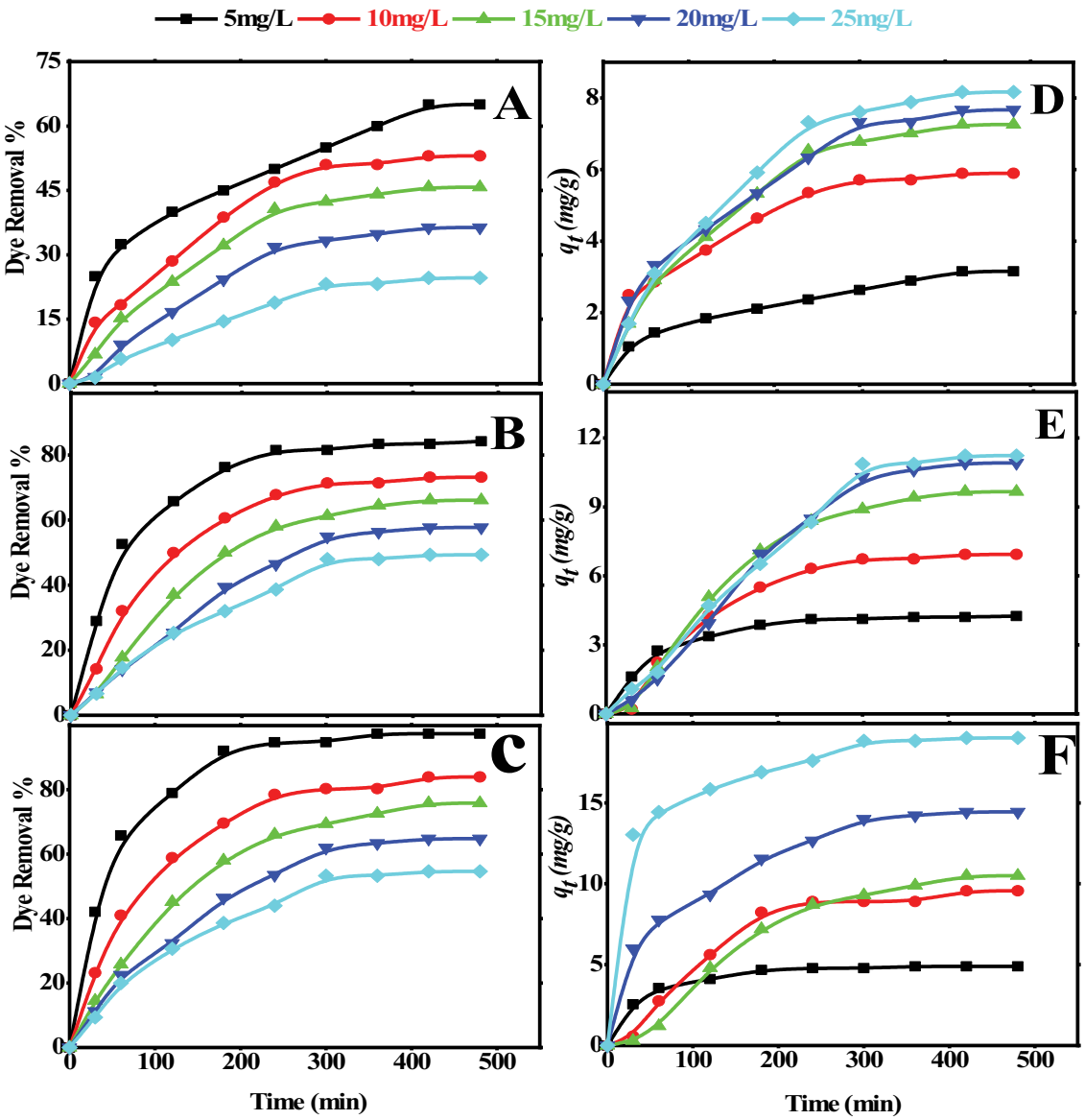

Fig. 3. Effect of CR dye concentration and contact time on the removal % and the amount of CR dye adsorbed at 25°C and pH 7 by 20 mg of (A,D) Z, (B,E) LF, and (C,F) ZLF.

on the surface of adsorbents and dye molecules in the bulk liquid phase is responsible for reduction rate in the CR dye adsorption [41]. Additionally, dye removal % was reduced as the initial CR dye concentration increased. The increased amount of dye absorbed by the adsorbent with raising the initial CR dye concentration is due to the greater driving force for mass transfer at a raised starting dye concentration.

General trend was noticed for all concentrations, the ZLF nano-composite revealed superior efficiency for Congo red adsorption, and the CR elimination percent was in the order ZLF > LF > Z. The more the initial CR concentration, the more the amount of CR adsorbed which may be interpretted by the evolution of the concentration gradient when the initial CR dye concentration rises, as seen in Fig. 3D–F. And hence, in increase in the driving force was noticed for the point which is sufficient enough to overcome the mass transfer resistance of the CR adsorbate as well as the Z, LF, and ZLF adsorbents [62,63]. At pH 7 and 25°C, the maximum adsorption capacities of ZLF were found to be 4.88, 9.56, 10.5, 14.4, and 19 mg/g for CR dye with initial concentrations of 5, 10, 15, 20, and 25 mg/L, respectively. In the same order, the maximum adsorption capacities for LF adsorbent were 4.25, 6.93, 9.66, 10.9, and 11.23 mg/g, while for Z adsorbent were 3.1, 5.9, 7.25, 7.6, and 8.1 mg/g. The results revealed that modification of Z pores and surface with LF is a viable method for improving Z's CR removal performance.

3.2.2. *Effect of adsorbent doses*

In order to determine the optimal adsorbent dosage for the greatest efficiency, the influence of adsorbent mass on Congo red dye removal efficiency was examined. Fig. 4A

demonstrates the amount of CR dye removed in percent as a function of adsorbent dose. The doses of adsorbent usually varied from 0.01 to 0.05 g. Fig. 4A demonstrates that the more the adsorbent dose increases from 0.01 to 0.05 g the more the dye removal efficiency. A general trend was noticed for all adsorbents where an increasing from 46.15% to 64.62% in the case of Z adsorbent, from 70.00% to 92.40% in the case of LF adsorbent, and from 80.00% to 97.60% in the case of ZLF adsorbent. This finding could be ascribed by the fact that as the adsorbent mass increases, so do the number of active sites [41,48,62,64]. In the case of ZLF and Z, increasing the adsorbent dose from 0.01 to 0.03 g results in a significant increase in removal efficiency. In the case of ZLF and Z, increasing the adsorbent dose over 0.03 g resulted in a minor change in the removal efficiency. The formation of a dense screening layer over the surface of the adsorbent which resulted from the accumulation of adsorbent particles and a reduction in the distance between the adsorbent molecules, known as the screening effect, which is familiar usually at higher adsorbent doses, could explain this phenomenon. The binding sites were hidden from CR molecules by the condensed layer on the adsorbent's surface. Additionally, due to Z and ZLF overlapping, CR molecules fight for a limited number of accessible binding sites. Agglomeration or aggregation at higher Z and ZLF dosages lengthens the diffusion channel for CR adsorption, lowering the adsorption rate [49,65,66] and it also led to the overall reduction in the sorbent–sorbate contact [64].

3.2.3. Effect of pH

The pH is considered one of the most important factors that regulates the CR dye removal capacitance of adsorbent during conducting a wastewater treatment. More and more, adsorption efficiency is well-controlled by controlling the pH of the solution under investigation as any variation in pH will be reflected directly on the ionization degree of the adsorptive molecules as well as the adsorbent surface

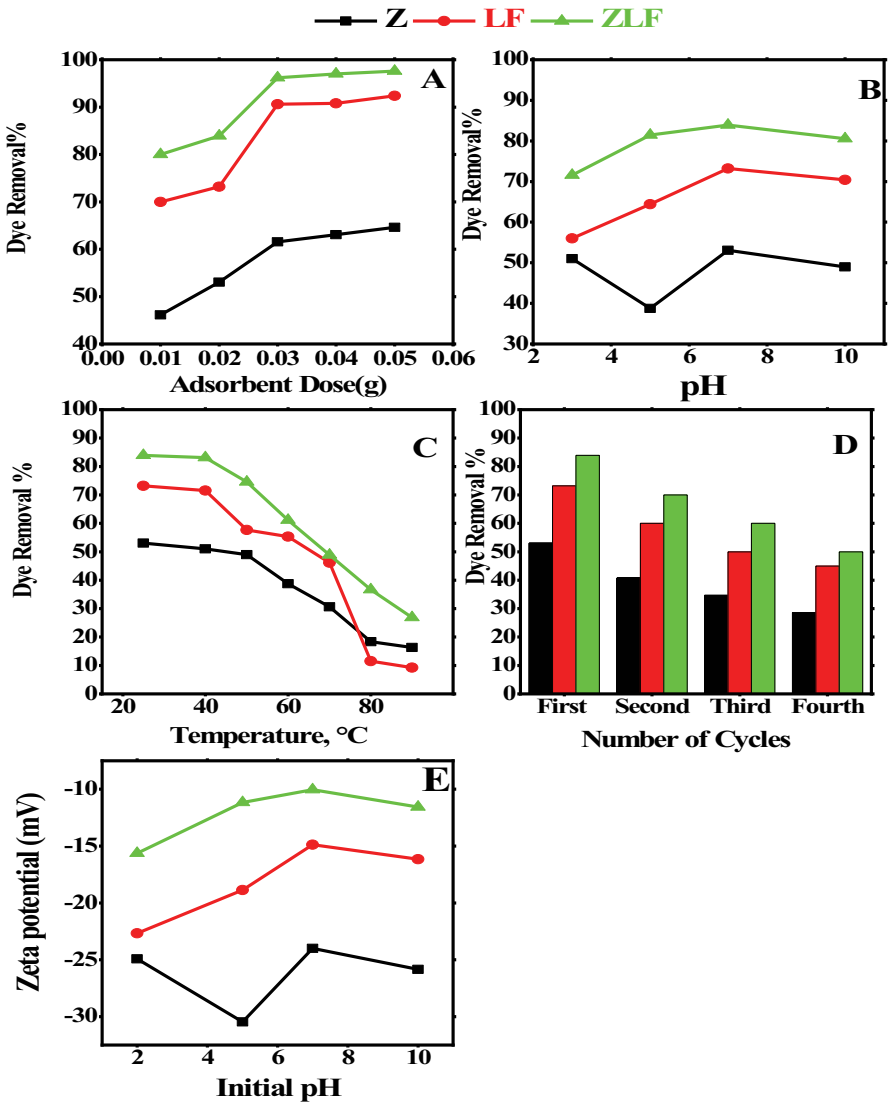

Fig. 4. Effect of (A) adsorbent dose, (B) initial pH of the solution, (C) adsorption temperature, (D) reusability test on the removal % of 20 mL CR solution of 10 mg/L by Z, LF, and ZLF, and (E) Zeta potential as a function of pH.

characteristics. The effect of pH on the percent of CR dye captured by the adsorbent is demonstrated in Fig. 4B. A pH range from 3 to 10 was investigated for the dye with an initial concentration of 10 mg/L, sorbent dosage 0.02 g of Z per 20 mL of CR solution. At pH values of 3, 5, 7, and 10, the Z adsorbent displays removal efficiency of 51.02%, 38.78%, 53.06%, and 48.98% respectively, while the LF adsorbent exhibits removal efficiency of 56.00%, 64.42%, 73.21%, and 70.40%, and finally the ZLF adsorbent shows removal efficiency of 71.56%, 81.45%, 83.93%, and 80.54%. Zeta potential of composites in the solution was evaluated, in order to investigate the effects on Z, LF, and ZLF. The effect of pH on the zeta potential of Z, LF, and ZLF in an aqueous solution was shown in Fig. 4E which revealed that Z, LF, and ZLF acquired a negative surface charge in the pH range of 2–10 and its zeta potential became less negative at higher pH values. The surface charge of Z, LF, and ZLF changed from lower to higher values as the pH value increased from 2 to 10, which resulted in a gradual increase in electrostatic attraction between the adsorbent and the negatively charged CR. In case Z, a larger fluctuation of adsorption capacity was observed at a pH ranging from 2 to 7 reflect a large change in zeta potential. Generally, the more the shift in the zeta potential value to the positive values the more the removal %. The lower zeta potential indicates that the adsorbents surface were partially negatively charged at a pH of 2 to 10 and that the electrostatic force between Z, LF, and ZLF and CR through the sulfonic acid group (SO_3^-) was mainly repulsive during the experiment [67,68]. On other words, when the system's pH increase, the population of negatively charged sites in the surface of adsorbent decreases, and the population of positively charged sites on the surface of adsorbent increases. So in higher pH, the A positively charged surface has a considerably high electrostatic interaction with anionic dyes that increase adsorption. Also, at lower pH, ionic repulsion between the negatively charged surface and the anionic dye molecules decreases adsorption [69]. The pH values at which the adsorbent has zero-point charge (pH_{zpc}) were not detected in case of Z, LF, and ZLF under the investigated pH ranges. The gradual increase of the adsorption capacity at pH from 2 and 10 in case of Z and ZLF adsorbent could be related to the shift on zeta potential to less negative values.

The irregular behavior of zeolite in zeta potential results could be ascribed by partial dissolution of zeolite components during the measurement followed by re-adsorption of dissolved species at elevated pH values as reported previously by Nosrati et al. [70]. Moreover, the lack of uniformity on zeolite surface which resulted in presence of various active sites with different strengths and chemical nature affected directly on values of zeta potential which lies in line with the data explained by Hasse et al. [71]. Much more explanation, the presence of multivalent cations like Al + 3 which upon leaching to the solution during measurement causes subsequent hydrolysis followed by precipitation on zeolite surface which alters surface free charges as well as ionic strength [70]. Finally, presence of alkali metals as well as SiO_2, Al_2O_3 ration in zeolite framework have their own contribution to the irregularity in zeta potential values as stated by Liu et al. [72].

3.2.4. Effect of temperature

Temperature effects on CR dye adsorption are another important physico-chemical parameter as it directly affects adsorption capabilities of the adsorbent's [73]. As it is clear from Fig. 4C, adsorption trials were conducted at temperatures of 25°C, 40°C, 50°C, 60°C, 70°C, 80°C, and 90°C. The more the temperature rises, the less the percentage of CR removed. This might be attributed to the fact that the adsorption forces diminishes between active binding sites of the adsorbent and the CR adsorbate species, which were responsible for the adsorption of CR dye molecules on the adsorbent surface [74–77]. And hence, 25°C is considered the temperature of choice for CR adsorption onto all investigated adsorbents. The adsorption of CR onto Z, LF, and ZLF is an exothermic reaction, as seen by the decrease in CR removal efficiency as temperature rises.

3.2.5. Reusability test

Fig. 4D demonstrates that the Z, LF, and ZLF re-usage tests for the removal of CR dye were repeated four times keeping the same conditions. The data obtained revealed that the removal capability of all utilized adsorbents varied across the four adsorption cycles. The recorded dye removal % was 53.06%@1st cycle, 40.82%@2nd cycle, 34.69%@3rd cycle, and 28.57%@4th cycle for Z while LF adsorbent recorded a decreased from 73.21%@1st cycle to 45.00@4th cycle, whereas ZLF nanoadsorbent recorded a decreased from 83.93%@1st cycle to 50.00%@4th cycle. The drop in CR removal efficiency could be related to the agglomeration of CR molecules on the surface of Z, LF, and ZLF adsorbents, which hinders the adsorbent surface and pores from dissolved CR molecules, resulting in a noticeable decrease in adsorption capacity [78].

3.3. Adsorption isotherm

The correlation coefficient known as statistical significance of R^2 was calculated from the linear plots of C_e/q_e vs. C_e, $\log(q_e)$ against $\log(C_e)$, and q_e against $\ln(C_e)$. This function was used to fit the data to Langmuir, Freundlich, and Temkin isotherms, respectively. The computed values of K_L, K_F, K_T, Q_o, n, B, and R^2 were derived from the linear plots in Fig. 5 and recorded in Table 1. Table 1 shows that CR adsorption on Z and LF adsorbents almost follows the Langmuir isotherm model with the highest R^2 value; the adsorption process almost follows the Langmuir isotherm model [22,79]. Accordingly, a multilayer adsorption process of CR dye molecules occurs at surface of the adsorbent especially at the active sites with uneven accessible heterogeneous sites, varied adsorption energies, and interactions between adsorbed molecules. At 25°C, the R^2 values calculated by the Langmuir isotherms of Z and LF adsorbents were 0.965 and 0.997 respectively. The value of R_L is less than one, indicating that CR adsorption in the studied case is advantageous [80]. The adsorption isotherm mechanism of CR onto ZLF was found to follow the Temkin isotherms after Z was replaced with LF to generate the ZLF composite. As a result, the dye is removed from a single surface layer at the active sites of ZLF adsorbents, and the adsorbed CR molecules do

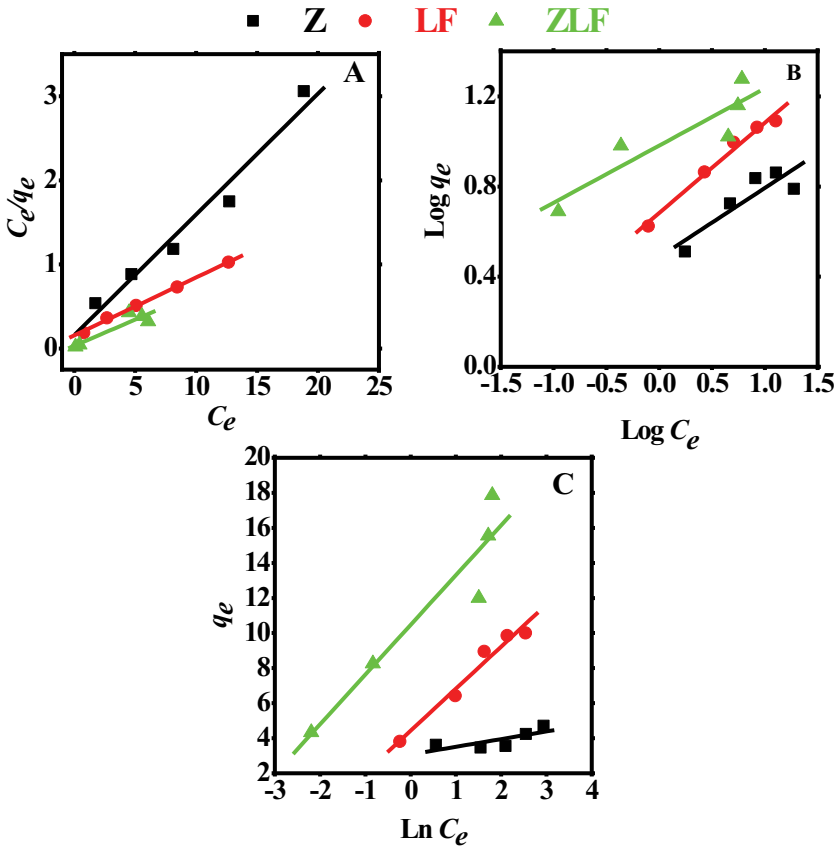

Fig. 5. Plots of (A) Langmuir, (B) Freundlich, and (C) Temkin adsorption isotherms for the adsorption of CR dye by 20 mg of Z, LF, and ZLF at 25°C and initial pH 7.

Table 1
Isotherm parameters for CR adsorption on Z, LF, and ZLF at 25°C and initial pH 7

Langmuir isotherm				
Constant / Adsorbent	Q_o (mg/g)	K_L (L/mg)	R_L	R^2
ZLF	16.07	1.88	0.10	0.851
LF	14.50	0.44	0.04	0.997
Z	6.96	0.89	0.12	0.965
Freundlich isotherm				
Constant / Adsorbent	1/*n*	K_F	R^2	
ZLF	0.25	9.58	0.815	
LF	0.40	4.81	0.982	
Z	0.30	3.06	0.777	
Temkin isotherm				
Constant / Adsorbent	*B* (J/mol)	K_T (L/mol)	R^2	
ZLF	2.84	40.02	0.892	
LF	2.39	6.33	0.968	
Z	2.21	2.70	0.936	

not react with one another. At 25°C, the R^2 value calculated by the Temkin isotherms of ZLF adsorbent was 0.892. The value of R_L is 1, indicating that in the study scenario, CR adsorption is beneficial [80]. This means that the adsorption process is preferred, the surface is heterogeneous, and there are fewer contacts between the adsorbed ions. It also means that CR adsorption happens via multi-molecular and multi-anchorage adsorption mechanisms [81,82].

3.4. Adsorption kinetics

Under varied beginning dye concentrations, the CR dye adsorption process on Z, LF, and ZLF was studied in order to determine the best effective adsorption kinetics model. Each of first-order, second-order, and Elovich kinetics linear graphs were represented by $\ln(q_e - q_t)$ vs. t, t/q_t vs. t and q_t vs. ln$t$, respectively, as demonstrated in Fig. 6. The adsorption kinetics parameters k_1, k_2, q_e, β, and α of the evaluation model in addition to R^2 were calculated from the linear graph and depicted in Table 2. The linear fit and regression coefficient values in Table 2 for all of the tested kinetic models revealed that CR adsorption onto Z is adequately handled by the second-order kinetics model at all dye concentrations which indicates chemical adsorption, and the chemical reaction is limiting the process [8,83]. This is also confirmed by the good approximation between the estimated q_e and experimental $q_{e,\exp}$ [84]. All dye concentrations

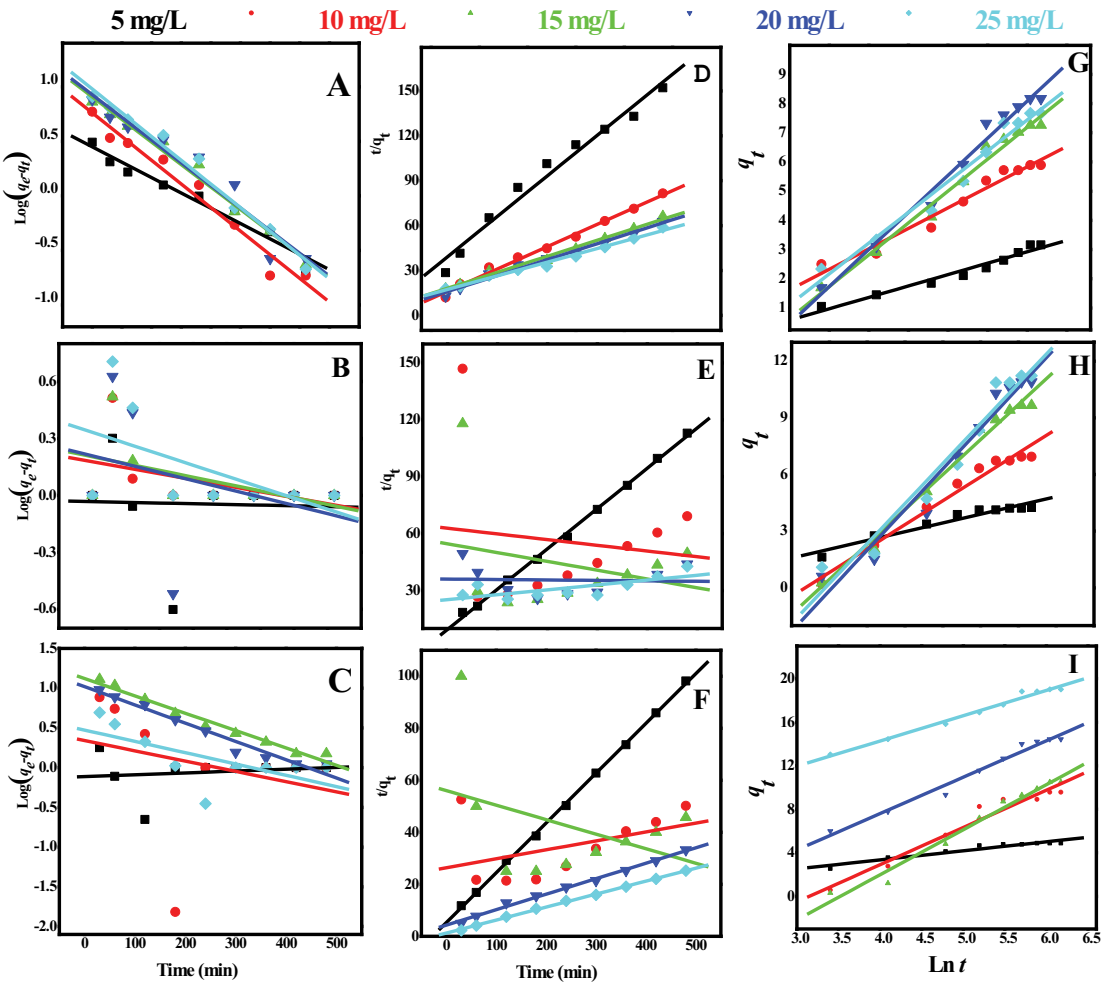

Fig. 6. (A–C) Pseudo-first-order, (D–F) pseudo-second-order, and (G–I) Elovich sorption kinetics of CR dye at 25°C and pH 7 by 20 mg of Z, LF, and ZLF, respectively.

Table 2
Parameters of the kinetic models for CR dye adsorption on Z, LF, and ZLF at 25°C and initial pH 7

Adsorbent	Conc., ppm	First-order				Second-order			Elovich kinetic model		
		$q_{e,exp}$	$q_{e,cal.}$	k_1	R^2	$q_{e,cal.}$	k_2	R^2	β (g/mg)	α (mg/min)	R^2
Z	5	3.10	2.75	0.0028	0.960	3.82	0.0023	0.975	1.316	0.08	0.959
	10	5.90	5.75	0.0043	0.968	6.94	0.0019	0.992	0.714	0.20	0.957
	15	7.25	7.95	0.0041	0.984	9.71	0.0007	0.992	0.454	0.14	0.983
	20	7.60	8.50	0.0042	0.935	9.80	0.0009	0.985	0.476	0.18	0.963
	25	8.10	9.50	0.0043	0.979	11.36	0.0006	0.989	0.385	0.15	0.983
LF	5	4.25	0.86	–0.0002	0.005	4.71	0.0047	0.824	1.079	0.25	0.939
	10	6.94	1.65	0.0014	0.337	–33.27	1.44E-5	0.887	0.395	0.11	0.973
	15	9.66	1.78	0.0016	0.415	–21.59	3.93E-5	0.930	0.270	0.13	0.984
	20	10.91	1.74	0.0017	0.135	58.16	0.00036	0.958	0.232	0.12	0.958
	25	11.23	2.59	0.003	0.488	38.91	2.62E-05	0.960	0.236	0.13	0.952
ZLF	5	4.89	0.77	–0.0005	0.023	5.22	4.889	0.813	1.204	0.86	0.932
	10	9.56	2.19	0.003	0.070	29.11	9.561	0.871	0.292	0.14	0.957
	15	10.50	13.22	0.005	0.974	–17.90	10.5	0.949	0.241	0.12	0.976
	20	14.44	10.45	0.005	0.960	16.79	14.44	0.957	0.299	0.59	0.978
	25	19.01	2.97	0.003	0.433	20.04	19.01	0.954	0.430	19.83	0.984

are efficiently handled by the Elovich kinetics model for CR adsorption onto LF and ZLF, demonstrating that adsorbent surfaces are not energetically homogenous.

3.5. Sorption mechanism

The experimental results were fitted for Weber's intraparticle diffusion kinetics model to recognize the CR dye adsorption process and rate-controlling Steps impacting adsorption kinetics. Fig. S2 shows a straight line in the chart of q_t vs. $t^{1/2}$. The values of the intraparticle propagation model rate constant (k_3) and border thickness constant (I) in Table 3 were calculated using the slope and intercept of the linear fitting of Fig. S2. The value of intercept I is not zero, indicating that the intraparticle diffusion model may not be the only rate-controlling mechanism in determining adsorption kinetics [85]. The boundary layer effect is reflected in the intercept in Fig. S2. The larger the intercept, the more important surface adsorption is in the rate control step [85].

3.6. Thermodynamic study

All thermodynamic parameters obtained from the adsorption process of CR dye onto Z, LF, and ZLF were demonstrated clearly in Fig. 7 and Table 4. Table 4 reveals that the negative values of ΔG indicates that the adsorption of the CR dye is spontaneous process and this noticeable shift in the value of ΔG to higher positive value at elevated temperature considered a proof that the adsorption process is not favorable at higher temperature. The values of ΔG at 298 K in this study are –0.3037, –2.4912, and –4.0953 for Z, LF, and ZLF adsorbents which found in the physical adsorption range of ΔG (ΔG for physical adsorption is in the range –20–0 kJ mol) revealing that the adsorption of CR dye onto Z, LF, and ZLF adsorbents is a physio-sorption process. This result is also confirmed by the "n" value that was determined by Freundlich isotherm model which is more than unity which refer to a physical adsorption process [86]. Also the value of R_L that falls in the range between 0 and 1, which indicate that the adsorption of dispersed red 60 dye is promising at the experimental conditions [80].

Table 3
Intraparticle diffusion constants for different initial CR concentrations at 25°C and initial pH 7

Adsorbent	Conc., ppm	Intraparticle diffusion kinetic model		
		I	k_3 (mg/g min$^{1/2}$)	R^2
Z	5	–1.60	0.589	0.912
	10	–0.50	0.505	0.946
	15	–1.50	0.514	0.886
	20	–0.10	0.357	0.956
	25	–0.60	0.191	0.895
LF	5	1.52	0.143	0.824
	10	–0.73	0.398	0.887
	15	–1.97	0.594	0.930
	20	–3.25	0.709	0.958
	25	–2.87	0.702	0.962
ZLF	5	2.47	0.128	0.813
	10	–0.89	0.539	0.871
	15	–2.93	0.673	0.949
	20	3.61	0.546	0.957
	25	11.53	0.377	0.954

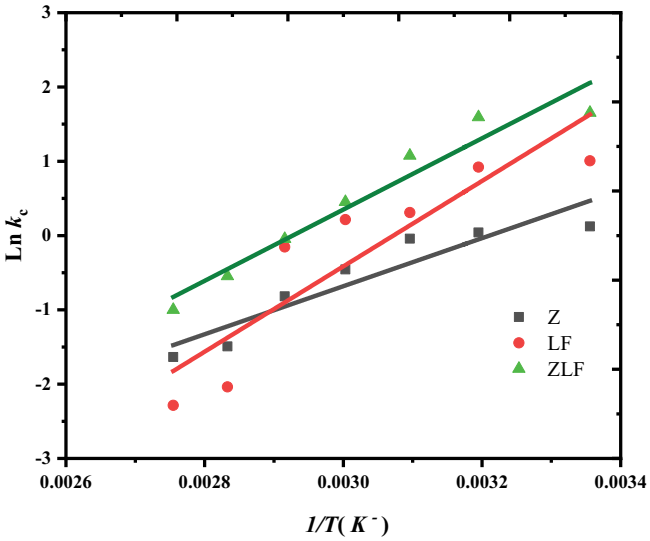

Fig. 7. Van't Hoff plot for CR dye adsorption onto Z, LF, and ZLF at initial pH 7.

Table 4
Thermodynamic parameters for adsorption of CR dye onto Z, LF, and ZLF

Adsorbents	Temperature (K)	ΔG (kJ/mol)	ΔH (kJ/mol)	ΔS (J/mol K)
Z	298	–0.3037	–26.87	–86.46
	313	–0.1062		
	323	0.10958		
	333	1.26451		
	343	2.33361		
	353	4.37784		
	363	4.93167		
LF	298	–2.4912	–47.75	–146.32
	313	–2.3984		
	323	–0.8329		
	333	–0.5955		
	343	0.43957		
	353	5.97806		
	363	6.89843		
ZLF	298	–4.0953	–39.87	–116.39
	313	–4.1468		
	323	–2.8877		
	333	–1.2513		
	343	0.12675		
	353	1.60398		
	363	3.01877		

Table 5
Comparison of the optimized conditions, removal %, and adsorption capacity of different CR adsorbents relative to our Z, LF, and ZLF nanoadsorbents

Adsorbent	Conditions	Adsorption capacity (mg/g)	Removal efficiency (%)	Reference
Ulva lactuca biomass	Contact time: 90 min; dose: 3 g; concentration: 100 mg/L ; pH: 7.0; temperature: 24°C	–	97.89%	[88]
Modified zeolite A (MZA)	Contact time: 120 min; dose: 3 g/L; concentration: 60 mg/L; pH: 6.0; temperature: 30°C	21.11	99.24%	[89]
Polyvinyl alcohol/sodium alginate/ZSM-5	Contact time: 180 min; dose: 1.875 g; concentration: 10–50 mg/L; pH: 3.0; temperature: 24°C	19.00	94.3%	[90]
Na-zeolite@chitosan	concentration: 800 ppm; pH: 5; time: 60 min	0.00428 mmol/g	98.019%	[91]
Cu(II)-incorporated zeolite Y	Dose: 1.5 g/L; concentration: 10 mg/L; temperature: 30°C	–	90%	[92]
ZLF	Contact time: 480 min; dose: 0.02 g; concentration:	19.01	97.37%	
LF	10 mg/L; pH: 7.0; temperature: 25°C	11.23	84.21%	This study
Z		8.1	65.00%	

The negative value ΔH proves that, the adsorption of CR dye onto Z, LF, and ZLF is an exothermic process. The –ve ΔS value indicates that the degree of randomness decreased at the solid/liquid interface due to CR dye adsorption onto Z, LF, and ZLF surfaces [87].

3.7. Field experiments

The newly manufactured nanoadsorbent, ZLF, was optimized with the following parameters: adsorbent weight (0.02 g), room temperature, no changes in the pH of the wastewater containing waste dye, and a contact period of 420 min. The presence of different wavelengths corresponding to different dyes was discovered by scanning wavelengths detected in the as-received industrial effluent. Absorbance at different wavelengths was measured at the end of the contact time to calculate the dyes' removal effectiveness from industrial effluent. The findings from the field testing showed that the newly synthesized nanoadsorbent was capable of extracting dyes from industrial wastewater with a 90.97% efficiency, confirming the foundation for new eco-friendly materials that aid in the reuse of industrial wastewater.

3.8. Comparison of adsorption capability of Z, LF, and ZLF with other adsorbents

Table 5 compares the adsorption capacity, q_m, and dye removal efficiency of various adsorbents reported in the literature with those of Z, LF, and ZLF for CR dye adsorption. It demonstrates that q_m values for various adsorbents vary significantly. In comparison to other adsorbents [88–92], the results showed that Z, LF, and ZLF had a satisfactory adsorption capability for CR dye from aqueous solutions.

4. Conclusion

Surface and in pores modification of Z and LF yielded a novel alga/zeolite composite ZLF, which was employed as a new adsorbent for CR dye from aqueous solutions. The experimental results demonstrated that decreasing the initial concentration of CR improved the removal efficiency of CR, and that the CR removal rate is high during the early stages of the adsorption experiment. By raising the dosage of Z, LF, and ZLF from 0.01 g to 0.05 g, the elimination percent rose. The temperature has a significant impact on the percentage of CR removed. Changing the initial pH of the CR solution from 3 to 10 affects the CR removal efficiency for all adsorbents, with maximum adsorption occurring at pH 7. The reusability test for Z, LF, and ZLF adsorbents revealed that none of them were preferred for CR removal reuse. The adsorption isotherms of CR onto Z, LF, and ZLF demonstrate that the Langmuir isotherm models are the best fit by Z and LF adsorbents, whereas the Temkin isotherm model is the best fit by ZLF. The Elovich model well handles CR adsorption onto LF and ZLF, while Z follows second-order kinetics. Finally, field tests demonstrated that the newly synthesized ZLF adsorbent had a 97.36% efficiency in removing dyes from industrial wastewater, confirming the basis of new eco-friendly materials that aid in the reuse of industrial wastewater. The thermodynamic results showed that the adsorption of the CR dye onto Z, LF, and ZLF is spontaneous and exothermic adsorption process.

References

[1] T.J. Al-Musawi, N. Mengelizadeh, O. Al Rawi, D. Balarak, Capacity and modeling of Acid Blue 113 Dye adsorption onto chitosan magnetized by Fe_2O_3 nanoparticles, J. Polym. Environ., 30 (2022) 344–359.
[2] T.J. Al-Musawi, P. Rajiv, N. Mengelizadeh, I.A. Mohammed, D. Balarak, Development of sonophotocatalytic process for degradation of Acid Orange 7 dye by using titanium dioxide nanoparticles/graphene oxide nanocomposite as a catalyst, J. Environ. Manage., 292 (2021) 112777, doi: 10.1016/j.jenvman.2021.112777.
[3] D. Balarak, F. Ganji, S.S. Choi, S.M. Lee, M.J. Shim, Effects of operational parameters on the removal of Acid Blue 25 dye from aqueous solutions by electrocoagulation, Appl. Chem. Eng., 30 (2019) 742–748.
[4] M. Sillanpää, A.H. Mahvi, D. Balarak, A.D. Khatibi, Adsorption of Acid orange 7 dyes from aqueous solution

using polypyrrole/nanosilica composite: experimental and modelling, Int. J. Environ. Anal. Chem., (2021) 1–18, doi: 10.1080/03067319.2020.1855338.
[5] H. Shayesteh, A. Rahbar-Kelishami, R. Norouzbeigi, Evaluation of natural and cationic surfactant modified pumice for Congo red removal in batch mode: kinetic, equilibrium, and thermodynamic studies, J. Mol. Liq., 221 (2016) 1–11.
[6] D. Balarak, H. Abasizadeh, J.-K. Yang, M.J. Shim, S.-M. Lee, Biosorption of Acid Orange 7 (AO7) dye by canola waste: equilibrium, kinetic and thermodynamics studies, Desal. Water Treat., 190 (2020) 331–339.
[7] Z. Xiong, H. Zheng, Y. Hu, X. Hu, W. Ding, J. Ma, Y. Li, Selective adsorption of Congo red and Cu(II) from complex wastewater by core-shell structured magnetic carbon@zeolitic imidazolate frameworks-8 nanocomposites, Sep. Purif. Technol., 277 (2021) 119053, doi: 10.1016/j.seppur.2021.119053.
[8] S.H. Mosavi, R. Zare-Dorabei, M. Bereyhi, Microwave-assisted synthesis of metal–organic framework MIL-47 for effective adsorptive removal of dibenzothiophene from model fuel, J. Iran. Chem. Soc., 18 (2021) 709–717.
[9] L. Liu, B. Zhu, G.-X. Wang, Azoxystrobin-induced excessive reactive oxygen species (ROS) production and inhibition of photosynthesis in the unicellular green algae *Chlorella vulgaris*, Environ. Sci. Pollut. Res., 22 (2015) 7766–7775.
[10] X.-q. Cao, X. Wang, M. Chen, F. Xiao, Y.-m. Huang, X.-j. Lyu, Synthesis of nanoscale zeolitic imidazolate framework-8 (ZIF-8) using reverse micro-emulsion for Congo red adsorption, Sep. Purif. Technol., 260 (2021) 118062, doi: 10.1016/j.seppur.2020.118062.
[11] M. Shaban, M.R. Abukhadra, Geochemical evaluation and environmental application of Yemeni natural zeolite as sorbent for Cd^{2+} from solution: kinetic modeling, equilibrium studies, and statistical optimization, Environ. Earth Sci., 76 (2017) 310, doi: 10.1007/s12665-017-6636-3.
[12] M. Shaban, F.A. Elwahab, A.E. Ghitas, M.Y. El Zayat, Efficient and recyclable photocatalytic degradation of methylene blue dye in aqueous solutions using nanostructured $Cd_{1-x}Co_xS$ films of different doping levels, J. Sol-Gel Sci. Technol., 95 (2020) 276–288.
[13] M. Shaban, H. Abdallah, L. Said Mahmoud, A.M. Ahmed, Water desalination and dyes separation from industrial wastewater by PES/TiO_2NTs mixed matrix membranes, J. Polym. Res., 26 (2019) 1–12, doi: 10.1007/s10965-019-1831-4.
[14] S. Kim, J.C. Muñoz-Senmache, B.-M. Jun, C.M. Park, A. Jang, M. Yu, A.J. Hernández-Maldonado, Y. Yoon, A metal organic framework-ultrafiltration hybrid system for removing selected pharmaceuticals and natural organic matter, Chem. Eng. J., 382 (2020) 122920, doi: 10.1016/j.cej.2019.122920.
[15] M.R. Rahman-Setayesh, A. Rahbar Kelishami, H. Shayesteh, Equilibrium, kinetic, and thermodynamic applications for methylene blue removal using Buxus sempervirens leaf powder as a powerful low-cost adsorbent, J. Part. Sci. Technol., 5 (2019) 161–170.
[16] H.M. El-Zeiny, M.R. Abukhadra, O.M. Sayed, A.H.M. Osman, S.A. Ahmed, Insight into novel β-cyclodextrin-grafted-poly(*N*-vinylcaprolactam) nanogel structures as advanced carriers for 5-fluorouracil: equilibrium behavior and pharmacokinetic modeling, Colloids Surf., A, 586 (2020) 124197, doi: 10.1016/j.colsurfa.2019.124197.
[17] A.Q. Selim, L. Sellaoui, S.A. Ahmed, M. Mobarak, E.A. Mohamed, A.B. Lamine, A. Erto, A. Bonilla-Petriciolet, M.K. Seliem, Statistical physics-based analysis of the adsorption of Cu^{2+} and Zn^{2+} onto synthetic cancrinite in single-compound and binary systems, J. Environ. Chem. Eng., 7 (2019) 103217, doi: 10.1016/j.jece.2019.103217.
[18] T. Van Tran, V. Dai Cao, V.H. Nguyen, B.N. Hoang, D.-V.N. Vo, T.D. Nguyen, L.G. Bach, MIL-53 (Fe) derived magnetic porous carbon as a robust adsorbent for the removal of phenolic compounds under the optimized conditions, J. Environ. Chem. Eng., 8 (2020) 102902, doi: 10.1016/j.jece.2019.102902.
[19] T. Van Tran, D.T.C. Nguyen, T.T. Nguyen, C. Van Nguyen, D.-V.N. Vo, T.D. Nguyen, High performance of $Mn_2(BDC)_2(DMF)_2$-derived MnO@C nanocomposite as superior remediator for a series of emergent antibiotics, J. Mol. Liq., 308 (2020) 113038, doi: 10.1016/j.molliq.2020.113038.
[20] M. Shaban, M.R. Abukhadra, M. Shahien, S.S. Ibrahim, Novel bentonite/zeolite-NaP composite efficiently removes methylene blue and Congo red dyes, Environ. Chem. Lett., 16 (2018) 275–280.
[21] D. Balarak, T.J. Al-Musawi, I.A. Mohammed, H. Abasizadeh, The eradication of reactive black 5 dye liquid wastes using *Azolla filiculoides* aquatic fern as a good and an economical biosorption agent, SN Appl. Sci., 2 (2020) 1015, doi: 10.1007/s42452-020-2841-x.
[22] S. Mohebali, D. Bastani, H. Shayesteh, Equilibrium, kinetic and thermodynamic studies of a low-cost biosorbent for the removal of Congo red dye: acid and CTAB-acid modified celery (*Apium graveolens*), J. Mol. Struct., 1176 (2019) 181–193.
[23] D. Sud, G. Mahajan, M. Kaur, Agricultural waste material as potential adsorbent for sequestering heavy metal ions from aqueous solutions–a review, Bioresour. Technol., 99 (2008) 6017–6027.
[24] M. Shaban, M.I. Sayed, M.G. Shahien, M.R. Abukhadra, Z.M. Ahmed, Adsorption behavior of inorganic-and organic-modified kaolinite for Congo red dye from water, kinetic modeling, and equilibrium studies, J. Sol-Gel Sci. Technol., 87 (2018) 427–441.
[25] A. Nasar, F. Mashkoor, Application of polyaniline-based adsorbents for dye removal from water and wastewater—a review, Environ. Sci. Pollut. Res., 26 (2019) 5333–5356.
[26] J. Tang, Y.-F. Zhang, Y. Liu, Y. Li, H. Hu, Efficient ion-enhanced adsorption of Congo red on polyacrolein from aqueous solution: experiments, characterization and mechanism studies, Sep. Purif. Technol., 252 (2020) 117445, doi: 10.1016/j.seppur.2020.117445.
[27] M. Liu, W. Yin, T.-L. Zhao, Q.-Z. Yao, S.-Q. Fu, G.-T. Zhou, High-efficient removal of organic dyes from model wastewater using $Mg(OH)_2$-MnO_2 nanocomposite: synergistic effects of adsorption, precipitation, and photodegradation, Sep. Purif. Technol., 272 (2021) 118901, doi: 10.1016/j.seppur.2021.118901.
[28] N. El Messaoudi, M. El Khomri, S. Bentahar, A. Dbik, A. Lacherai, B. Bakiz, Evaluation of performance of chemically treated date stones: application for the removal of cationic dyes from aqueous solutions, J. Taiwan Inst. Chem. Eng., 67 (2016) 244–253.
[29] M. Kumar, R. Gokulan, S. Sujatha, S.P.S. Priya, S. Praveen, S. Elayaraja, Biodecolorization of Reactive Red 120 in batch and packed bed column using biochar derived from *Ulva reticulata*, Biomass Convers. Biorefin., (2021) 1–15, doi: 10.1007/s13399-020-01268-x.
[30] R. Sabarish, G. Unnikrishnan, Polyvinyl alcohol/carboxymethyl cellulose/ZSM-5 zeolite biocomposite membranes for dye adsorption applications, Carbohydr. Polym., 199 (2018) 129–140.
[31] M. Abukhadra, M. Shaban, Recycling of different solid wastes in synthesis of high-order mesoporous silica as adsorbent for safranin dye, Int. J. Environ. Sci. Technol., 16 (2019) 7573–7582.
[32] S. Alaya-Ibrahim, A. Kovo, A. Abdulkareem, O. Adeniyi, M.D. Yahya, Development of nano-silver doped zeolite A synthesized from Nigerian Ahoko kaolin for treatment of wastewater of a typical textile company, Chem. Eng. Commun., 207 (2020) 1114–1137.
[33] M.S. Mirqasemi, M. Homayoonfal, M. Rezakazemi, Zeolitic imidazolate framework membranes for gas and water purification, Environ. Chem. Lett., 18 (2020) 1–52.
[34] R. Sabarish, G. Unnikrishnan, Synthesis, characterization and evaluations of micro/mesoporous ZSM-5 zeolite using starch as bio template, SN Appl. Sci., 1 (2019) 1–13.
[35] S. Radoor, J. Karayil, A. Jayakumar, J. Parameswaranpillai, S. Siengchin, Efficient removal of methyl orange from aqueous solution using mesoporous ZSM-5 zeolite: synthesis, kinetics and isotherm studies, Colloids Surf., A, 611 (2021) 125852, doi: 10.1016/j.colsurfa.2020.125852.
[36] J. Zhou, F. Zheng, H. Li, J. Wang, N. Bu, P. Hu, J.-m. Gao, Q. Zhen, S. Bashir, J.L. Liu, Optimization of post-treatment variables to produce hierarchical porous zeolites from coal gangue to enhance adsorption performance, Chem. Eng. J., 381 (2020) 122698, doi: 10.1016/j.cej.2019.122698.

[37] D. Verboekend, J. Pérez-Ramírez, Design of hierarchical zeolite catalysts by desilication, Catal. Sci. Technol., 1 (2011) 879–890.
[38] Y. Wang, T. Yokoi, S. Namba, T. Tatsumi, Effects of dealumination and desilication of beta zeolite on catalytic performance in *n*-hexane cracking, Catalysts, 6 (2016) 8, doi: 10.3390/catal6010008.
[39] M. Khedr, M. Nasr, K. Abdel Halim, A. Farghali, N. Soliman, Catalytic decomposition of hydrocarbon gas over various nanostructured metal oxides for hydrocarbon removal and production of carbon nanotubes, Int. J. Eng. Res. Gen. Sci, 2 (2014) 413.
[40] M. Shaban, M. Mustafa, A. El Sayed, Structural, optical, and photocatalytic properties of the spray deposited nanoporous CdS thin films; influence of copper doping, annealing, and deposition parameters, Mater. Sci. Semicond. Process., 56 (2016) 329–343.
[41] N. Khamis Soliman, A.F. Moustafa, A.A. Aboud, K.S.A. Halim, Effective utilization of *Moringa* seeds waste as a new green environmental adsorbent for removal of industrial toxic dyes, J. Mater. Res. Technol., 8 (2019) 1798–1808.
[42] R. Nodehi, H. Shayesteh, A. Rahbar-Kelishami, Fe_3O_4@NiO core–shell magnetic nanoparticle for highly efficient removal of Alizarin red S anionic dye, Int. J. Environ. Sci. Technol., 19 (2022) 2899–2912.
[43] M.H. Khedr, K.S. Abdel Halim, N.K. Soliman, Synthesis and photocatalytic activity of nano-sized iron oxides, Mater. Lett., 63 (2009) 598–601.
[44] F. Mohamed, M.R. Abukhadra, M. Shaban, Removal of safranin dye from water using polypyrrole nanofiber/Zn-Fe layered double hydroxide nanocomposite (Ppy NF/Zn-Fe LDH) of enhanced adsorption and photocatalytic properties, Sci. Total Environ., 640 (2018) 352–363.
[45] H. Freundlich, Over the adsorption in solution, J. Phys. Chem., 57 (1906) 1100–1107.
[46] M. Temkin, Kinetics of ammonia synthesis on promoted iron catalysts, Acta Physiochim. URSS, 12 (1940) 327–356.
[47] O. Ozdemir, B. Armagan, M. Turan, M.S. Celik, Comparison of the adsorption characteristics of azo-reactive dyes on mezoporous minerals, Dyes Pigm., 62 (2004) 49–60.
[48] N. Soliman, H.S. Mohamed, R.H. Elsayed, N.M. Elmedny, A.H. Elghandour, S.A. Ahmed, Removal of chromium and cadmium ions from aqueous solution using residue of *Rumex dentatus* L. plant waste, Desal. Water Treat., 149 (2019) 181–193.
[49] H.S. Mohamed, N.K. Soliman, D.A. Abdelrheem, A.A. Ramadan, A.H. Elghandour, S.A. Ahmed, Adsorption of Cd^{2+} and Cr^{3+} ions from aqueous solutions by using residue of *Padina gymnospora* waste as promising low-cost adsorbent, Heliyon, 5 (2019) e01287, doi: 10.1016/j.heliyon.2019.e01287.
[50] N.K. Soliman, H.S. Mohamed, S.A. Ahmed, F.H. Sayed, A.H. Elghandour, S.A. Ahmed, Cd^{2+} and Cu^{2+} removal by the waste of the marine brown macroalga *Hydroclathrus clathratus*, Environ. Technol. Innovation, 15 (2019) 100365, doi: 10.1016/j.eti.2019.100365.
[51] M. Gougazeh, J.-C. Buhl, Synthesis and characterization of zeolite A by hydrothermal transformation of natural Jordanian kaolin, J. Assoc. Arab Univ. Basic Appl. Sci., 15 (2014) 35–42.
[52] M.M. Treacy, J.B. Higgins, Collection of Simulated XRD Powder Patterns for Zeolites Fifth, 5th Revised Edition, Elsevier, Allentown, PA, USA, 2007.
[53] Z. Pi, Z. Liu, C. Yang, X. Tian, J. Fei, J. Zheng, Exfoliation of kaolinite by urea-intercalation precursor and microwave irradiation assistance process, Front. Earth Sci. China, 1 (2007) 26–29.
[54] L. Vaculikova, E. Plevova, S. Vallova, I. Koutnik, Characterization and differentiation of kaolinites from selected Czech deposits using infrared spectroscopy and differential thermal analysis, Acta Geodyn. Geomater., 8 (2011) 59–67.
[55] E. Horvath, J. Kristof, R.L. Frost, Vibrational spectroscopy of intercalated kaolinites. Part I, Appl. Spectrosc. Rev., 45 (2010) 130–147.
[56] J. Madejova, P. Komadel, Baseline studies of the clay minerals society source clays: infrared methods, Clays Clay Miner., 49 (2001) 410–432.
[57] R. Masoudi, H. Moghimi, E. Azin, R.A. Taheri, Adsorption of cadmium from aqueous solutions by novel Fe_3O_4-newly isolated *Actinomucor* sp. bio-nanoadsorbent: functional group study, Artif. Cells Nanomed. Biotechnol., 46 (2018) S1092–S1101.
[58] P. Nautiyal, K. Subramanian, M. Dastidar, Adsorptive removal of dye using biochar derived from residual algae after in-situ transesterification: alternate use of waste of biodiesel industry, J. Environ. Manage., 182 (2016) 187–197.
[59] M. Ruthiraan, E. Abdullah, N. Mubarak, M. Noraini, A promising route of magnetic based materials for removal of cadmium and methylene blue from wastewater, J. Environ. Chem. Eng., 5 (2017) 1447–1455.
[60] M.M. Ghoneim, H.S. El-Desoky, K.M. El-Moselhy, A. Amer, E.H. Abou El-Naga, L.I. Mohamedein, A.E. Al-Prol, Removal of cadmium from aqueous solution using marine green algae, *Ulva lactuca*, Egypt. J. Aquat. Res., 40 (2014) 235–242.
[61] W.M. Ibrahim, A.F. Hassan, Y.A. Azab, Biosorption of toxic heavy metals from aqueous solution by *Ulva lactuca* activated carbon, Egypt. J. Basic Appl. Sci., 3 (2016) 241–249.
[62] H.S. Mohamed, N.K. Soliman, A.F. Moustafa, O.F. Abdel-Gawad, R.R. Taha, S.A. Ahmed, Nano metal oxide impregnated chitosan-4-nitroacetophenone for industrial dye removal, Int. J. Environ. Anal. Chem., 101 (2021) 1850–1877.
[63] Y.C. Sharma, Optimization of parameters for adsorption of methylene blue on a low-cost activated carbon, J. Chem. Eng. Data, 55 (2010) 435–439.
[64] D. Balarak, M. Zafariyan, C.A. Igwegbe, K.K. Onyechi, J.O. Ighalo, Adsorption of Acid Blue 92 dye from aqueous solutions by single-walled carbon nanotubes: isothermal, kinetic, and thermodynamic studies, Environ. Processes, 8 (2021) 869–888.
[65] M. Asif Tahir, H.N. Bhatti, M. Iqbal, Solar Red and Brittle Blue direct dyes adsorption onto *Eucalyptus angophoroides* bark: equilibrium, kinetics and thermodynamic studies, J. Environ. Chem. Eng., 4 (2016) 2431–2439.
[66] A. Kanwal, H.N. Bhatti, M. Iqbal, S. Noreen, Basic dye adsorption onto clay/$MnFe_2O_4$ composite: a mechanistic study, Water Environ. Res., 89 (2017) 301–311.
[67] C. Jiang, X. Wang, B. Hou, C. Hao, X. Li, J. Wu, Construction of a lignosulfonate–lysine hydrogel for the adsorption of heavy metal ions, J. Agric. Food Chem., 68 (2020) 3050–3060.
[68] W. Zhang, Y. Lan, M. Ma, S. Chai, Q. Zuo, K.-H. Kim, Y. Gao, A novel chitosan–vanadium-titanium-magnetite composite as a superior adsorbent for organic dyes in wastewater, Environ. Int., 142 (2020) 105798, doi: 10.1016/j.envint.2020.105798.
[69] S.H. Mosavi, R. Zare-Dorabei, M. Bereyhi, Rapid and effective ultrasonic-assisted adsorptive removal of Congo red onto MOF-5 modified by $CuCl_2$ in ambient conditions: adsorption isotherms and kinetics studies, ChemistrySelect, 6 (2021) 4432–4439.
[70] A. Nosrati, J. Addai-Mensah, W. Skinner, pH-mediated interfacial chemistry and particle interactions in aqueous muscovite dispersions, Chem. Eng. J., 152 (2009) 406–414.
[71] B. Hasse, J. Gläsel, A.M. Kern, D.Y. Murzin, B.J.M. Etzold, Preparation of carbide-derived carbon supported platinum catalysts, Catal. Today, 249 (2015) 30–37.
[72] X. Liu, P. Mäki-Arvela, A. Aho, Z. Vajglova, V.M. Gun'ko, I. Heinmaa, N. Kumar, K. Eränen, T. Salmi, D.Y. Murzin, Zeta potential of beta zeolites: influence of structure, acidity, pH, temperature and concentration, Molecules, 23 (2018) 946, doi: 10.3390/molecules23040946.
[73] J. Zhang, Q. Zhou, L. Ou, Kinetic, isotherm, and thermodynamic studies of the adsorption of methyl orange from aqueous solution by chitosan/alumina composite, J. Chem. Eng. Data, 57 (2012) 412–419.
[74] S. Noreen, H.N. Bhatti, M. Zuber, M. Zahid, M. Asgher, Removal of Actacid Orange-RL dye using biocomposites: modeling studies, Pol. J. Environ. Stud., 26 (2017) 2125–2134.
[75] M. Mushtaq, H.N. Bhatti, M. Iqbal, S. Noreen, *Eriobotrya japonica* seed biocomposite efficiency for copper adsorption: isotherms, kinetics, thermodynamic and desorption studies, J. Environ. Manage., 176 (2016) 21–33.
[76] A. Rashid, H.N. Bhatti, M. Iqbal, S. Noreen, Fungal biomass composite with bentonite efficiency for nickel and zinc adsorption: a mechanistic study, Ecol. Eng., 91 (2016) 459–471.

[77] H.S. Mohamed, N.K. Soliman, A.F. Moustafa, O.F. Abdel-Gawad, R.R. Taha, S.A. Ahmed, Nano metal oxide impregnated chitosan-4-nitroacetophenone for industrial dye removal, Int. J. Environ. Anal. Chem., 101 (2019) 1850–1877.
[78] A. Naghizadeh, Regeneration of carbon nanotubes exhausted with humic acid using electro-Fenton technology, Arabian J. Sci. Eng., 41 (2016) 155–161.
[79] S. Nazerdeylami, R. Zare-Dorabei, Simultaneous adsorption of Hg^{2+}, Cd^{2+} and Cu^{2+} ions from aqueous solution with mesoporous silica/DZ and conditions optimise with experimental design: kinetic and isothermal studies, Micro Nano Lett., 14 (2019) 823–827.
[80] K.R. Hall, L.C. Eagleton, A. Acrivos, T. Vermeulen, Pore-and solid-diffusion kinetics in fixed-bed adsorption under constant-pattern conditions, Ind. Eng. Chem. Fundam., 5 (1966) 212–223.
[81] S. Bagherifam, S. Komarneni, A. Lakzian, A. Fotovat, R. Khorasani, W. Huang, J. Ma, S. Hong, F.S. Cannon, Y. Wang, Highly selective removal of nitrate and perchlorate by organoclay, Appl. Clay Sci., 95 (2014) 126–132.
[82] L. Sellaoui, H. Guedidi, S. Knani, L. Reinert, L. Duclaux, A.B. Lamine, Application of statistical physics formalism to the modeling of adsorption isotherms of ibuprofen on activated carbon, Fluid Phase Equilib., 387 (2015) 103–110.
[83] M. Bereyhi, R. Zare-Dorabei, S.H. Mosavi, Microwave-assisted synthesis of CuCl-MIL-47 and application to adsorptive denitrogenation of model fuel: response surface methodology, ChemistrySelect, 5 (2020) 14583–14591.
[84] R. Nodehi, H. Shayesteh, A.R. Kelishami, Enhanced adsorption of Congo red using cationic surfactant functionalized zeolite particles, Microchem. J., 153 (2020) 104281, doi: 10.1016/j.microc.2019.104281.
[85] W.J. Weber Jr., J.C. Morris, Kinetics of adsorption on carbon from solution, J. Sanit. Eng. Div., 89 (1963) 31–59.
[86] A.S. Özcan, B. Erdem, A. Özcan, Adsorption of Acid Blue 193 from aqueous solutions onto BTMA-bentonite, Colloids Surf., A, 266 (2005) 73–81.
[87] S. Yadav, V. Srivastava, S. Banerjee, C.-H. Weng, Y.C. Sharma, Adsorption characteristics of modified sand for the removal of hexavalent chromium ions from aqueous solutions: kinetic, thermodynamic and equilibrium studies, Catena, 100 (2013) 120–127.
[88] N.E.-A. El-Naggar, N.H. Rabei, S.E. El-Malkey, Eco-friendly approach for biosorption of Pb^{2+} and carcinogenic Congo red dye from binary solution onto sustainable *Ulva lactuca* biomass, Sci. Rep., 10 (2020) 1–22.
[89] I.H. Khalaf, F.T. Al-Sudani, A.A. AbdulRazak, T. Aldahri, S. Rohani, Optimization of Congo red dye adsorption from wastewater by a modified commercial zeolite catalyst using response surface modeling approach, Water Sci. Technol., 83 (2021) 1369–1383.
[90] S. Radoor, J. Karayil, J. Parameswaranpillai, S. Siengchin, Removal of anionic dye Congo red from aqueous environment using polyvinyl alcohol/sodium alginate/ZSM-5 zeolite membrane, Sci. Rep., 10 (2020) 1–15.
[91] Y. Yulizar, T. Utari, D. Apriandanu, Y. Putri, Chitosan nanoparticles on a natural zeolite as an efficient adsorbent for Congo red, IOP Conf. Ser.: Mater. Sci. Eng., 496 (2019) 012005.
[92] S. Chowdhury, K.G. Bhattacharyya, Use of Cu(II)-incorporated zeolite Y for decolourization of dyes in water: a case study with aqueous methylene blue and Congo red, SN Appl. Sci., 1 (2019) 87, doi: 10.1007/s42452-018-0094-8.

Supporting information

S1. Adsorption isotherms

Langmuir, Freundlich, and Temkin isotherms have been applied to explain the reaction isotherm of the designed Z, *Liagora farinosa* (LF), and zeolite/algae (ZLF) nanocomposite for the tested Congo red. The three models can be represented by Eqs. (S1)–(S3), respectively [1–4]:

$$\frac{C_e}{q_e} = \frac{1}{K_L Q_o} + \frac{C_e}{Q_o} \tag{S1}$$

$$\log q_e = \log K_F + \frac{1}{n}\log C_e \tag{S2}$$

$$q_e = B\ln K_T + B\ln C_e \tag{S3}$$

where, Q_o is the maximum amount of dye removed by Z, LF and ZLF adsorbents (mg/g); K_L, K_F, and K_T indicate to Langmuir constant, Freundlich constant, and Temkin binding constant, respectively. $B(=RT/b)$ is a constant associated with the adsorbed heat, n is the adsorption density, T is the absolute temperature, and R is the universal gas constant.

S2. Adsorption kinetics and mechanism

Different adsorption mechanisms and kinetics models such as intraparticle diffusion, pseudo-first-order, pseudo-second-order, and simple Elovich kinetic model are used for identifying the adsorption mechanisms and kinetics models that best match with the adsorption of Congo red onto Z, LF and ZLF adsorbents.

Eqs. (4)–(7) are used to represent the pseudo-first-order, pseudo-second-order, simple Elovich kinetic, and intraparticle diffusion models, respectively [5–11].

$$\ln\left(q_e - q_t\right) = \ln q_e - k_1 t \tag{S4}$$

$$\frac{t}{q_t} = \frac{1}{k_2 q_e^2} + \frac{t}{q_e} \tag{S5}$$

$$q_t = \frac{1}{\beta}\ln\alpha\beta + \frac{1}{\beta}\ln t \tag{S6}$$

$$q_t = k_3 t^{1/2} + I \tag{S7}$$

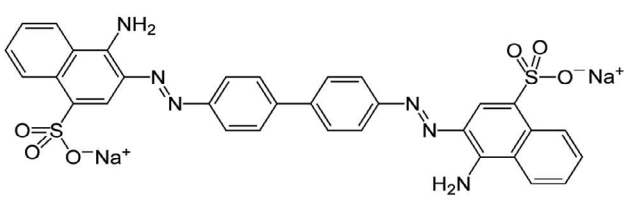

Fig. S1. Structure of Congo red.

where k_1, k_2, and k_3 represent rate constants of the pseudo-first-order, pseudo-second-order, and intraparticle propagation models. I refers to a constant related to the boundary thickness. α implies the adsorption rate at time = 0 min (mg/min) and β represents the extent of surface coverage (g/mg).

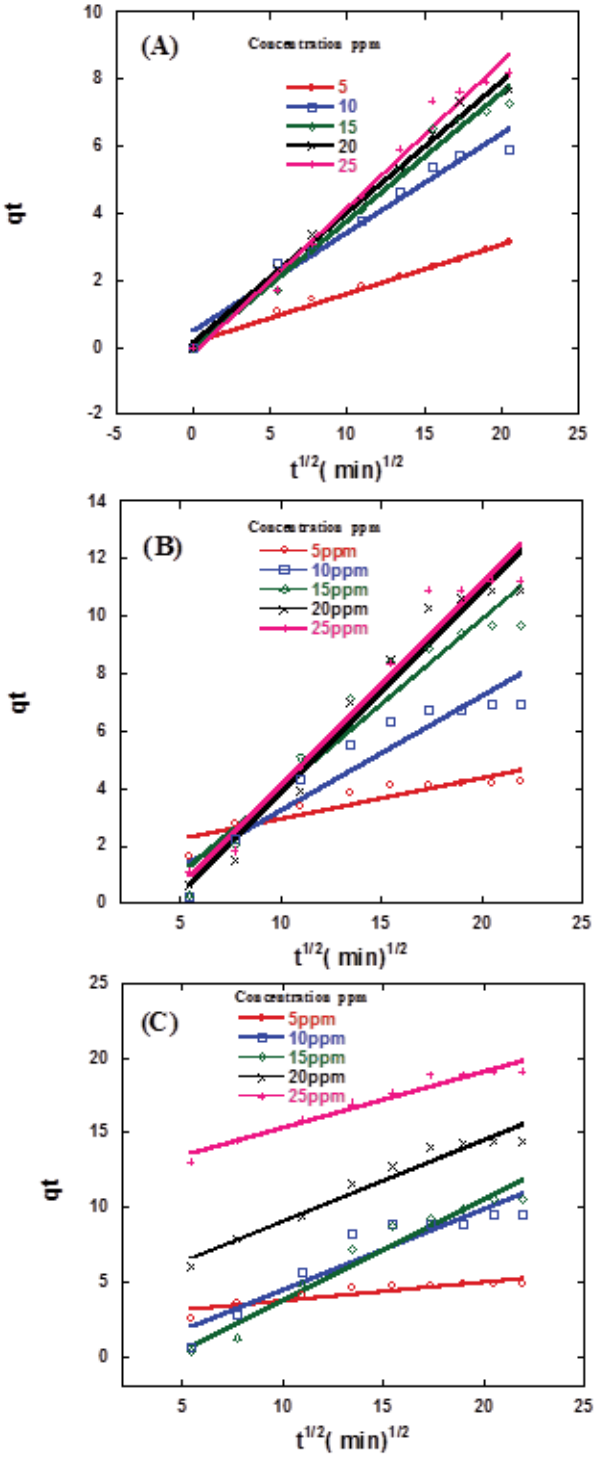

Fig. S2. Intraparticle sorption kinetics of Congo red dye at 25°C and pH 7 by 20 mg of (A) Z, (B) LF, and (C) ZLF.

S3. Characteristic wavenumbers and function groups of FTIR bands for Z, LF and ZLF adsorbents

FTIR peaks (cm^{-1})			Assignment	References
Z	LF	ZLF		
–	3,700	3,300–3,500	Amine group (–NH) stretching	[12]
3,452; 3,432 and 3,442	3,422	2,915	Hydroxyl group (–OH)	[13–15]
–	2,935	1,475	(–CH) group	[16,17]
–	1,647	1,069	(–C=O) group	[18]
1,029	–	1,039	Si–O–Al	[19]
464	–	471	Si–O–Si bending	[20]
400–800	–	400–800	Metal oxides	[21]

Table S1
Conditions of experimental adsorption tests

Series	Dye concentration, ppm	Z, LF and ZLF weight, g	Temperature, °C	pH value
1	5, 10, 15, 20 and 25	0.02	25	7
2	10	0.01, 0.02, 0.03, 0.04 and 0.05	25	7
3	10	0.02	40, 50, 60,70, 80 and 90	7
4	10	0.02	25	3, 4, 5, 7, 8 and 10

S1. References

[S1] I. Langmuir, The adsorption of gases on plane surfaces of glass, mica and platinum, J. Am. Chem. Soc., 40 (1918) 1361–1403.

[S2] H. Freundlich, Over the adsorption in solution, J. Phys. Chem., 57 (1906) 1100–1107.

[S3] K. Foo, B.H. Hameed, Insights into the modeling of adsorption isotherm systems, Chem. Eng. J., 156 (2010) 2–10.

[S4] M. Temkin, V. Pyzhev, Kinetics of ammonia synthesis on promoted iron catalysts, Acta Physiochim. URSS, 12 (1940) 217–222.

[S5] N. Soliman, H.S. Mohamed, R.H. Elsayed, N.M. Elmedny, A.H. Elghandour, S.A. Ahmed, Removal of chromium and cadmium ions from aqueous solution using residue of *Rumex dentatus* L. plant waste, Desal. Water Treat., 149 (2019) 181–193.

[S6] N. Xin, X. Gu, H. Wu, Y. Hu, Z. Yang, Application of genetic algorithm-support vector regression (GA-SVR) for quantitative analysis of herbal medicines, J. Chemom., 26 (2012) 353–360.

[S7] H.S. Mohamed, N.K. Soliman, D.A. Abdelrheem, A.A. Ramadan, A.H. Elghandour, S.A. Ahmed, Adsorption of Cd^{2+} and Cr^{3+} ions from aqueous solutions by using residue of *Padina gymnospora* waste as promising low-cost adsorbent, Heliyon, 5 (2019) e01287, doi: 10.1016/j.heliyon.2019.e01287.

[S8] L. Fan, C. Luo, M. Sun, H. Qiu, X. Li, Synthesis of magnetic β-cyclodextrin–chitosan/graphene oxide as nanoadsorbent and its application in dye adsorption and removal, Colloids Surf., B, 103 (2013) 601–607.

[S9] H. Demiral, G. Gündüzoğlu, Removal of nitrate from aqueous solutions by activated carbon prepared from sugar beet bagasse, Bioresour. Technol., 101 (2010) 1675–1680.

[S10] N.K. Soliman, H.S. Mohamed, S.A. Ahmed, F.H. Sayed, A.H. Elghandour, S.A. Ahmed, Cd^{2+} and Cu^{2+} removal by the waste of the marine brown macroalga *Hydroclathrus clathratus*, Environ. Technol. Innovation, 15 (2019) 100365, doi: 10.1016/j.eti.2019.100365.

[S11] F.-C. Wu, R.-L. Tseng, R.-S. Juang, Initial behavior of intraparticle diffusion model used in the description of adsorption kinetics, Chem. Eng. J., 153 (2009) 1–8.

[S12] W.M. Ibrahim, A.F. Hassan, Y.A. Azab, Biosorption of toxic heavy metals from aqueous solution by *Ulva lactuca* activated carbon, Egypt. J. Basic Appl. Sci., 3 (2016) 241–249.

[S13] R.L. Frost, E. Horváth, É. Makó, J. Kristóf, Modification of low-and high-defect kaolinite surfaces: implications for kaolinite mineral processing, J. Colloid Interface Sci., 270 (2004) 337–346.

[S14] Z. Pi, Z. Liu, C. Yang, X. Tian, J. Fei, J. Zheng, Exfoliation of kaolinite by urea-intercalation precursor and microwave irradiation assistance process, Front. Earth Sci. China, 1 (2007) 26–29.

[S15] L. Vaculikova, E. Plevova, S. Vallova, I. Koutnik, Characterization and differentiation of kaolinites from selected Czech deposits using infrared spectroscopy and differential thermal analysis, Acta Geodyn. Geomater., 8 (2011) 59–67.

[S16] P. Nautiyal, K. Subramanian, M. Dastidar, Adsorptive removal of dye using biochar derived from residual algae after in-situ transesterification: alternate use of waste of biodiesel industry, J. Environ. Manage., 182 (2016) 187–197.

[S17] M. Ruthiraan, E. Abdullah, N. Mubarak, M. Noraini, A promising route of magnetic based materials for removal of cadmium and methylene blue from wastewater, J. Environ. Chem. Eng., 5 (2017) 1447–1455.

[S18] M.M. Ghoneim, H.S. El-Desoky, K.M. El-Moselhy, A. Amer, E.H. Abou El-Naga, L.I. Mohamedein, A.E. Al-Prol, Removal of cadmium from aqueous solution using marine green algae, *Ulva lactuca*, Egypt. J. Aquat. Res., 40 (2014) 235–242.

[S19] E. Horvath, J. Kristof, R.L. Frost, Vibrational spectroscopy of intercalated kaolinites. Part I, Appl. Spectrosc. Rev., 45 (2010) 130–147.

[S20] J. Madejova, P. Komadel, Baseline studies of the clay minerals society source clays: infrared methods, Clays Clay Miner., 49 (2001) 410–432.

[S21] R. Masoudi, H. Moghimi, E. Azin, R.A. Taheri, Adsorption of cadmium from aqueous solutions by novel Fe_3O_4-newly isolated *Actinomucor* sp. bio-nanoadsorbent: functional group study, Artif. Cells Nanomed. Biotechnol., 46 (2018) S1092–S1101.